Arch. Metall. Mater. **69** (2024), 4, 1473-1480

DOI: https://doi.org/10.24425/amm.2024.151417

LI ZHANG[1*], NAN LI[1]

ENHANCED MECHANICAL PROPERTIES OF Mg-8Li DUAL-PHASE ALLOY PROCESSED BY FRICTION STIRRING VERSUS HOT-EXTRUSION

The microstructure evolution, texture and tensile properties of the Mg-8Li dual-phase alloys processed by hot-extrusion and friction stir processing were investigated. It was found that the friction stir processing was more advantageous when compared with hot-extrusion in achieving the superior mechanical properties. The tensile strength, yield strength and elongation of the as-FSPed alloy reached 235.4 MPa, 185.3 MPa and 35.6%, respectively. The outstanding strength-ductility combination of the as-FSPed Mg-8Li alloy was ascribed to refined grains, weakened texture and formation of high-fraction high angle grain boundaries.

Keywords: Microstructure; mechanical property; Mg-8%Li alloy; hot-extrusion; friction stir processing

1. Introduction

As the lightest structural materials, Mg-Li dual-phase alloys (density of 1.35-1.65 g/cm^3) have drawn much attention in fields of aerospace, lightweight weapons, automobile and portable equipment [1,2]. In this alloy system, the plastic deformation ability of the alloys can be improved with the help of the β-Li phase with body centered cubic (BCC) crystal structure when the content of Li is greater than 5.5 wt.% [3,4]. However, the strength of the Mg-Li dual-phase alloys will decrease with increasing β-Li phase content. The low strength and poor cold-formability of Mg-Li alloys have limited seriously their further applications [5,6].

It is known that in order to improve the mechanical properties of Mg-base alloys, strengthening mechanisms such as solution strengthening, second phase strengthening and fine grain strengthening have been applied in the past several decades [7-11]. The alloying method and severe plastic deformation methods have been accepted as the two main approaches in realizing the strengthening effects. Among the severe plastic deformation methods, the friction stir processing (FSP) method was regarded as the most promising microstructural modification technique for Mg-base alloys, Al-based alloys and other alloys [12-14]. Nonetheless, the effects of FSP on the microstructure, grain, texture and mechanical properties of Mg-Al-Zn alloys have only been extensively investigated [15-17]. By contrast, there were limit investigations involving the effect of FSP on the dual-phase Mg-Li alloy systems [18-20]. Submicron scale and homogeneously mixed α-Mg and β-Li were obtained in dual-phase Mg-Li alloy treated by FSP [21], which showed the significant effect of the FSP on dual-phase Mg-Li alloys. In practice, hot extrusion was a common method for the processing of Mg-Li alloys [22,23]. Comparative analysis of the microstructure and mechanical properties of the alloy between the two processes is beneficial for the improvement of the mechanical properties on Mg-Li alloys. Therefore, in the present work, the as-cast Mg-8wt.%Li(Mg-8Li) dual-phase alloy was processed by hot extrusion and FSP, respectively. And the texture, microstructural evolution and mechanical properties of the resultant alloys processed using these two techniques were examined and thus some associated conclusions were drawn.

2. Experimental procedure

The Mg-8Li alloy was prepared from pure magnesium and Li ingots using a graphite crucible in an electric resistance furnace under mixed LiCl-LiF atmosphere. Prior to melting, all ingots were cleaned, dried, and then put into the crucible. The melt was held at 750°C for 30 min, poured into a graphite mold that was preheated to 200°C, and then cooled in air. A cast billet with a diameter of 100 mm was obtained. Then, the billet was annealed at 400°C for 4h for microstructure homogenization.

[1] SHENYANG AEROSPACE UNIVERSITY, SHENYANG, SCHOOL OF MATERIALS SCIENCE AND ENGINEERING, CHINA

* Corresponding author: zhangli@sau.edu.cn

Prior to hot working, the annealed billet was cut into two pieces. One part of the billet was extruded at 300°C in an extrusion ratio of 12.75:1 at an extrusion rate of 1 $mm \cdot s^{-1}$. The remainder was machined into sheets with the dimensions of 150 mm × 80 mm × 8 mm for the FSP. The hot-extrusion and the FSP were performed by using a reducing die and an FSW-3LM-4012 machine, respectively as schematically illustrated in Fig. 1. Both the hot-extrusion and the FSP were only performed one pass on corresponding alloys in this experiment. The FSP tool shoulder used in processing was made of hardened H13 steel, while the tool pin was made of tungsten carbide. The pin diameter, length, and shoulder diameter were 5, 3, and 15 mm, respectively. The pin was fully sunk in the Mg-8Li plate and made the shoulder just fully touch its surface. The advancing angle was 2° with respect to the vertical axis. The rotation speed was 800 rpm, and the corresponding processing speed was 2.5 $mm \cdot s^{-1}$. The processed samples were water quenched immediately at room temperature, and were named as the "as-FSPed" state.

The samples for microstructural observation, EBSD and mechanical testing were cut along the extruded direction (ED) or along the friction stir processed direction (FSPD) as shown in Fig. 1(c)-(d). An Olympus GX71 optical microscope (OM) was used for microstructure observation. Prior to observation, the samples were carefully ground, polished and etched with a solution of 10% HCl + 90% ethanol. Phase identification was carried out by X-ray diffraction (XRD) with Cu K_α radiation. Uniaxial tensile tests were conducted using a MTS Landmark electro-hydraulic servo testing system at a strain rate of $1\times10^{-3}s^{-1}$ at room temperature. Rectangular tensile samples with gauge dimensions of 15 × 5 × 2 mm^3 (length × width × thickness) were machined from the extruded bar and the as-FSPed plate. All of the samples were pulled until failure, and the data were recorded and plotted as engineering stress versus engineering strain. In order to ensure the reproducibility of properties, each tensile test was conducted three times. Each datum was the average of three tests. The engineering strain was calculated through measuring the gauge length of the samples' before and after tensile test. The fracture surfaces were also observed using a Zeiss Sigma HV type scanning electron microscope (SEM) in the secondary electron mode. The micro-orientation was analyzed using a Nordlys Nano EBSD system equipped on the SEM.

3. Results

3.1. Microstructure of the as-cast alloy

Fig. 2 showed the OM and XRD pattern of the Mg-8Li alloy in as-cast state. It was clear that the microstructure was composed of bright and gray zones. According to the obtained XRD pattern presented in Fig. 2(b) and the results of previous work [24], the bright and the gray zones were α-Mg phase and β-Li phase, respectively. The diameter of α-Mg was approximately 150 μm while the β-Li phases were smaller and distributed evenly among the α-Mg phases as shown in Fig. 2(a).

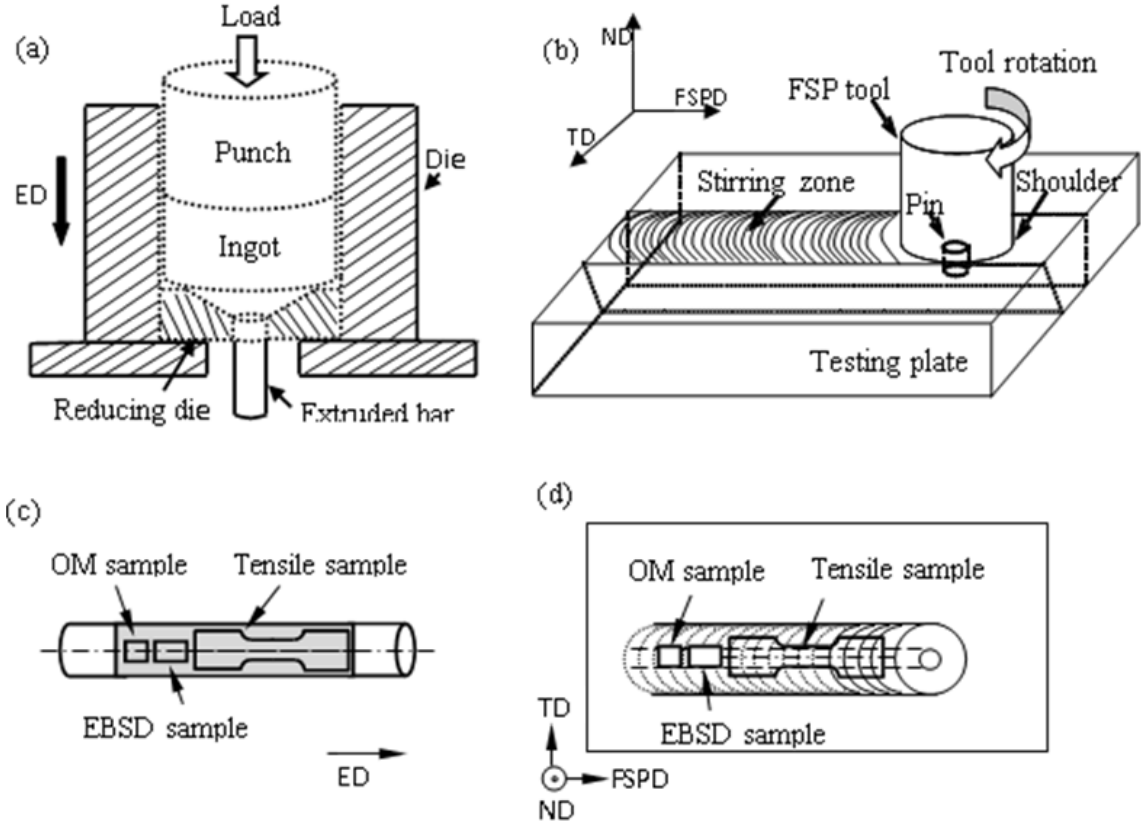

Fig. 1. Schematic illustration of process and sampling position: (a) hot-extrusion process, (b) friction stir process (FSP), (c) sampling position in hot-extrusion bar, (d) sampling position in as-FSPed plate

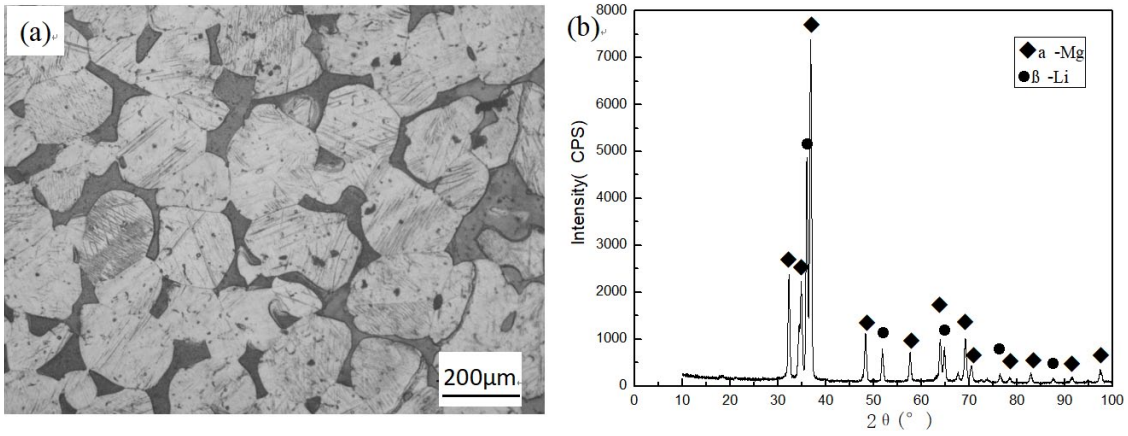

Fig. 2. Microstructure (a) and (b) XRD pattern of the as-cast Mg-8Li alloy

3.2. Microstructure of the processed Mg-8Li alloy

Fig. 3(a)-(c) were the microstructures of the Mg-8Li alloy processed by hot-extrusion and friction stir processes. Compared to the as-cast alloy (Fig. 2(a)), both processing methods could effectively refine the microstructure. After extrusion, both α-Mg and β-Li grains became smaller and were elongated along the ED as shown in Fig. 3(a). In particular, most of the β-Li phases became long strips, indicating that the alloy experienced severe deformation during the hot-extrusion process. Moreover, many small grains could be appeared among the non-equiaxed grains, indicating that dynamic recrystallization occurred during the extrusion. On the contrast, both α-Mg and β-Li grains became extremely fine after FSP as shown in Fig. 3(b). The average size of the grains was about 2 μm as shown in the magnified view of 'A' zone in Fig. 3(c).

EBSD results showed that the grain boundaries mainly consisted of low angular grain boundary (LAGB, $2° \leq \theta < 15°$) and only a small fraction of high angular grain boundary (HAGB, $\theta > 15°$) were observed in the as-extruded alloy as indicated by red and blue lines, respectively in Fig. 4(a)-(b). If the grain boundary angles exceed 15°, the grains were considered to be recrystallized, and if the grain boundary angles lower than 15° they were considered as the un-recrystallized regions. As for the as-FSPed one, most grain boundaries are composed of HAGBs, indicating that recrystallization was almost completed.

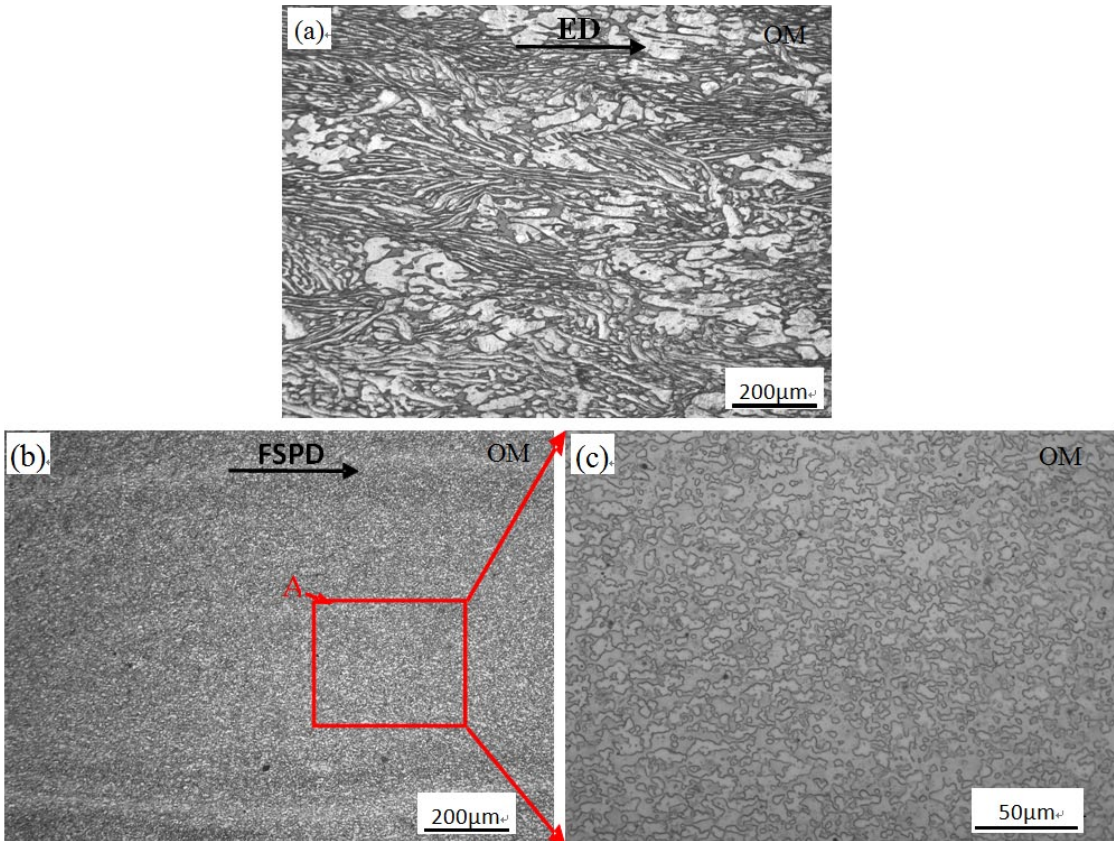

Fig. 3. Microstructure of the Mg-8Li alloy (a) as-extruded, (b)as-FSPed and (c) magnification of 'A' region

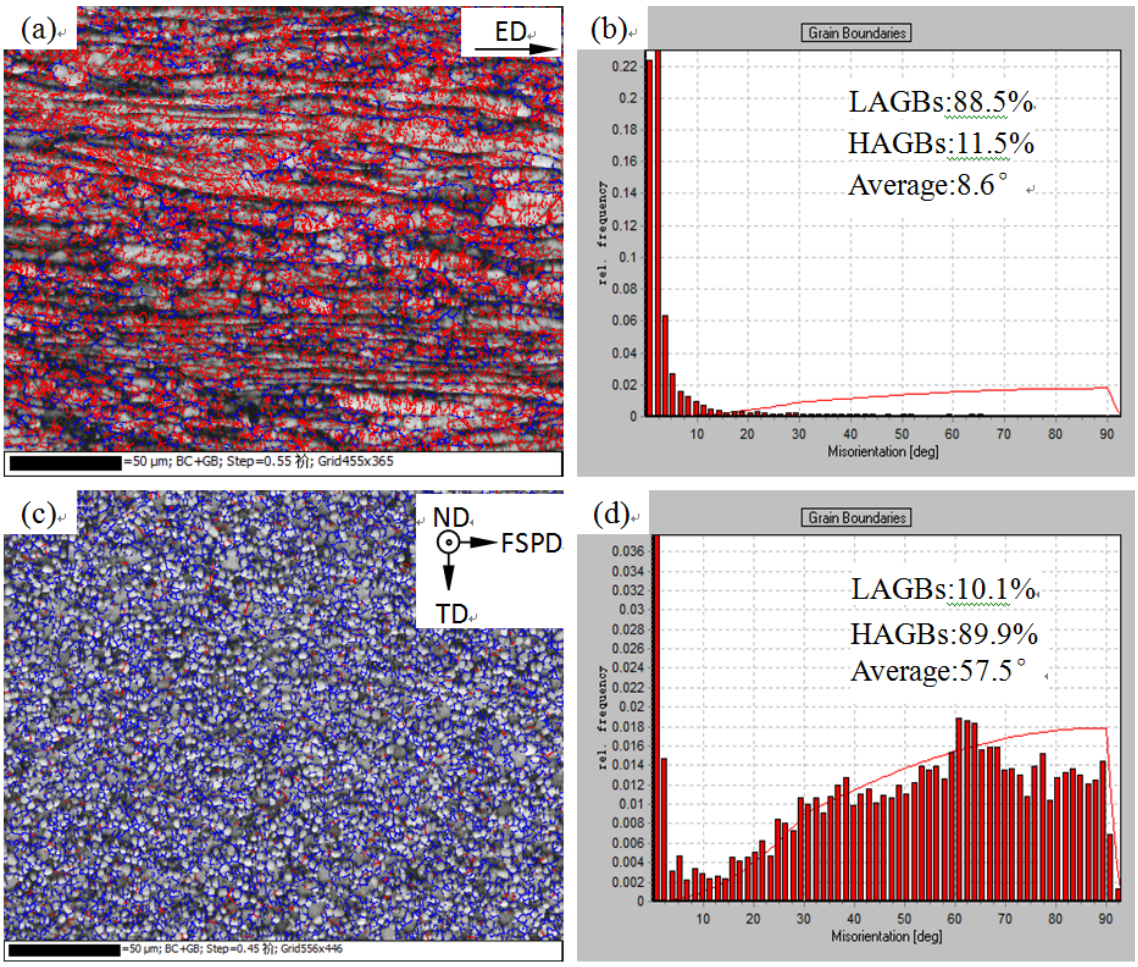

Fig. 4. Grain boundaries maps (red lines for LAGBs and blue lines for HAGBs) and misorientation distribution of the grain boundaries of the processed Mg-8Li alloys (a)-(b) as-extruded and (c)-(d) as-FSPed

As shown in Fig. 5, the grain size distributions of the two processed alloys were quite different. The grain size distribution of the as-extruded alloys was broad and the average grain size was estimated to be 10 μm (Fig. 5(a)), while the grain size distribution of the as-FSPed alloys was narrow and the average grain size was estimated to be 2 μm (Fig. 5(b)). It is clear that the FSP method is highly advantageous in grain refinement. This is consistent with the previous reports on other alloys [12-14].

3.3. Mechanical properties

Fig. 6 showed the typical tensile strain-stress curves of the samples under different processing conditions at room temperature. After processing, the tensile properties of the alloy were superior to those of the cast alloy. The yield strength (YS), ultimate tensile strength (UTS), and elongation (EL) of the as-extruded alloy reached 127.6 MPa, 189.7 MPa and 23.5%, respectively.

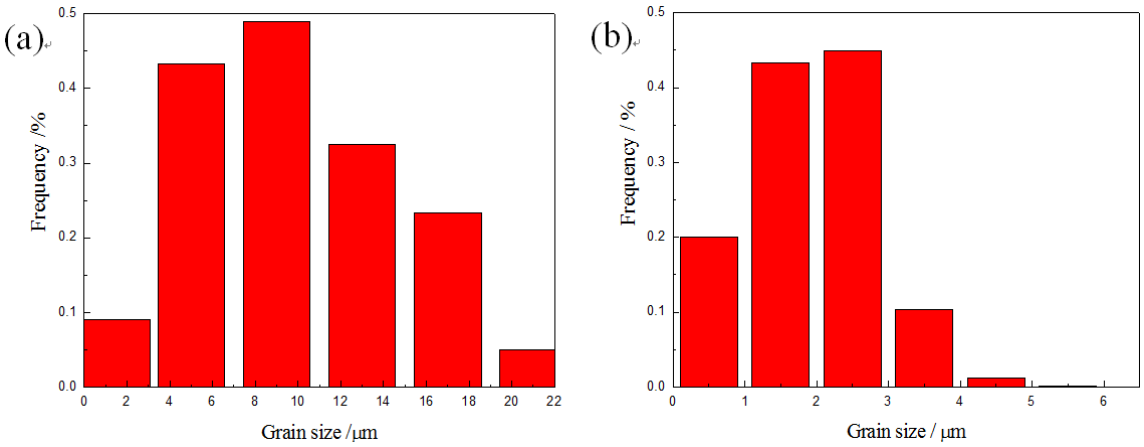

Fig. 5. Grain size distributions of the Mg-8Li alloy (a) as-extruded and (b) as-FSPed

The UTS and EL are about 1.5 times higher than those of the as-cast alloy, and the YS is 2.5 times higher than that of the as-cast one. Further, the as-FSPed alloys showed superior performance with respect to the as-extruded samples. The YS, UTS and EL of the as-FSPed alloy reached 185.3 MPa, 235.4 MPa and 35.6%, respectively. TABLE 1 showed the typical tensile properties data of the alloy under different conditions.

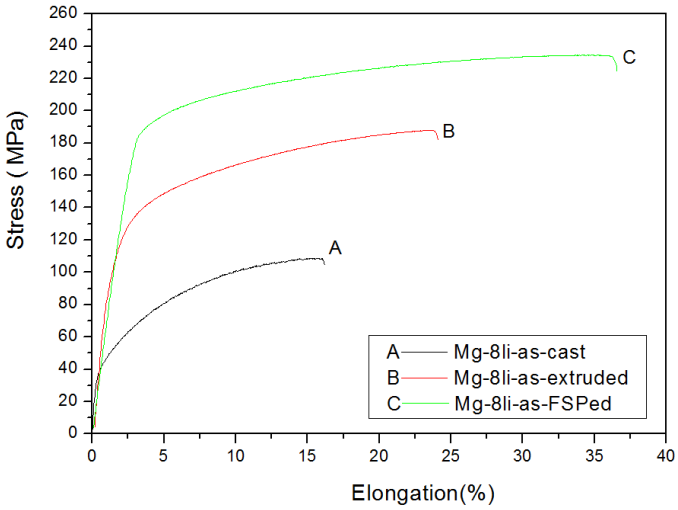

Fig. 6. Tensile strain-stress curves of the Mg-8Li alloy at different conditions

TABLE 1

Tensile properties of the Mg-8Li alloy at different conditions

Samples	Ultimate tensile strength (MPa)	Yield strength (MPa)	Elongation (%)
As-cast	109.8	48.6	16.2
As-extruded	189.7	127.6	23.5
As-FSPed	235.4	185.3	35.6

4. Discussions

Compared with the as-cast alloy, the as-extruded and the as-FSPed alloys exhibit a much finer grain size due to the dynamic recrystallisation that occurs during extrusion and friction stir process. The refined α-Mg and β-Li grains produce a large increase in strength and elongation for the two processed alloys [21]. It is of great interests to observe that with respect to the as-extrusion alloy, both the strength and ductility of the Mg-8%Li alloy were increased significantly after the FSP. Owing to the refined microstructure after the FSP, the traditional Hall-Petch (HP) relationship i.e. $\sigma_{ys} = \sigma_0 + k_y d^{-0.5}$, the correlation between the yield strength (σ_{ys}) and average grain size (d) becomes the first consideration to evaluate the strengthening effect. EBSD results showed that the grain boundaries mainly consisted of two kinds of grain boundaries: low angular grain boundary (LAGB, $2° \le \theta < 15°$) and high angular grain boundary (HAGB, $\theta > 15°$) for the Mg-8Li alloy after hot-extrusion and the FSP. The contribution of LAGB and HAGB to the increase of the yield stress is different owing to their different hindering capacity to the activated dislocations during the plastic straining process. Thus, in such a case, a modified HP relationship is given as following Eq. (1).

$$\sigma_{ys} = \sigma_0 + \sigma_{LAGB} + \sigma_{HAGB} \tag{1}$$

Where σ_{LAGB} and σ_{HAGB} present the strengthening contributions from LAGBs and HAGBs.

The contribution of HAGBs to strengthening follows the HP Eq. (2).

$$\sigma_{HAGB} = k_y (d/f)^{-1/2} \tag{2}$$

where f is the number fraction of HAGBs, and the statistic value of the as-extruded and as-FSPed are 11.5% and 89.9%, respectively as shown in Fig. 4(b)-(d).

Based on the research of literature [25], the value of k_y was estimated to be 50 MPa·μm$^{0.5}$ under the tension with the strain rate of 10^{-3}s^{-1}. Therefore, the increase of yield stress owing to the refined grains (HAGBs) with the mean size from as-extruded state (10 μm) to as-FSPed state (2 μm) was calculated to be 28.2 MPa.

The contribution of LAGBs to yield strength of as-processed samples can be evaluated by the dislocation strengthening mechanism, since the LAGB mainly consists of dislocations. The dislocation strengthening effect can be correlated with the dislocation density as following Eq. (3).

$$\sigma_{LAGB} = M\alpha Gb(\rho_0 + \rho_{LAGB})^{1/2} \tag{3}$$

where M is the average Taylor factor (i.e., ~2.5 in present case with strong fiber texture) [26], α is a constant (=0.2), G is the shear modulus (17 GPa), b is the Burgers vector of the gliding dislocations (0.32 nm), ρ_0 is the dislocation density estimated from the well-annealed materials ($\rho_0 \le 10^{12}$ m^2), ρ_{LAGB} is the dislocation located in the LAGBs.

The change in fraction of LAGBs under different processing conditions would necessarily result in variations of the dislocation density, and ρ_{LAGB} can be estimated by Eq. (4) according to Ref. [27].

$$\sigma_{LAGB} = 3(1-f)\bar{\theta}_{LAGB}/bd \tag{4}$$

Where f is still the number fraction of HAGBs, and $\bar{\theta}_{LAGB}$ is the average misorientation of LAGBs. $\bar{\theta}_{LAGB}$ is evaluated from the misorientation distribution data (misorientation *vs*. number fraction, as shown in Fig. 4), as illustrated in Ref. [27]. As a result, contribution from LAGBs to strengthening can be given as Eq. (5).

$$\sigma_{LAGB} = M\alpha Gb\left[\rho_0 + \frac{3(1-f)\bar{\theta}_{LAGB}}{bd}\right]^{1/2} \tag{5}$$

According to the Eq. (5), the increase of yield stress from as-extrusion state to as-FSPed state of the alloy owing to the LAGBs could be estimated to be: 1.414 × 68-0.586 × 68 = 34 MPa.

Hence, the increase of yield stress from as-extrusion state to as-FSPed state of the alloy could be calculated to be 62.2 MPa,

which was equal to the value 57.7 MPa measured by tension test. Therefore, it is concluded that the strengthening effect from the evolution of LAGBs and HAGBs during the processes of hot-extrusion and friction stir is the main underlying mechanism for the increase of yield stress of the Mg-Li alloy. And the extremely fine grains and high fraction of HAGBs play leading role in effectively improving the as-FSPed alloys' strength.

As to the increase of ductility after the FSP, the texture modification needs to be considered. Fig. 7 showed inverse pole figure (IPF) maps and {0001} pole figures of the as-extruded and as-FSPed alloys. After extrusion, most grains were shown in blue, indicating that the <01-10> direction was parallel to the extruded direction (Fig. 6(a)). A very sharp basal texture of the as-extruded alloys was observed in Fig. 7(c) and the magnitude of texture reaches 23.16. By contrast, the grains in the as-FSPed alloys were shown in different colors (Fig. 7(b)) because the texture of the alloys was random and its magnitude was only 4.21 (Fig. 7(d)). This indicates that the basal planes of most grains are not parallel to the processing direction. The random texture in the as-FSPed alloys is the main mechanism responsible for the increased ductility of the alloy. Furthermore, the texture evolution of β-Li would influence the ductility of the alloy [20], which is worth further studying.

Fig. 8 presents fracture morphologies of the Mg-8Li alloys under different conditions after tensile deformation. Typical cleavage fracture morphologies of the as-cast Mg-8Li alloy are shown in Fig. 8(a). Many cleavage planes with different orientations in the fracture were observed, and a few dimples could be found at the borders of these cleavage planes. After extrusion, some cleavage planes were still found in the fracture morphologies of the alloys as observed in Fig. 8(b). However, the surfaces of these cleavage planes were not smooth and the ridges of these cleavage planes showed tearing. Dimples with different depth were distributed in the fracture surface, and their number increased significantly. This suggests that the fracture mechanism of the Mg-8Li alloy was a mixture of brittle fracture and partial dimple ductile fracture. For the as-FSPed alloys (Fig. 8(c)), a large number dimples with different sizes were widely distributed in the fracture surfaces of the alloy, showing typical ductile fracture characteristics. The presence of these dimples provides evidence for high ductility of the as-FSPed Mg-8Li alloy.

5. Conclusions

In this work, dual-phase Mg-8Li alloy was processed by hot-extrusion and the FSP, respectively. It was found that both of these techniques could effectively improve the properties of Mg-8Li alloy. And some main conclusions can be made as follows:

(1) The YS, UTS, and EL of the as-extruded alloy reached 127.6 MPa, 189.7 MPa and 23.5%, respectively. The UTS and EL are about 1.5 times higher than those of the as-cast alloy, and the YS is 2.5 times higher than that of the as-cast one.

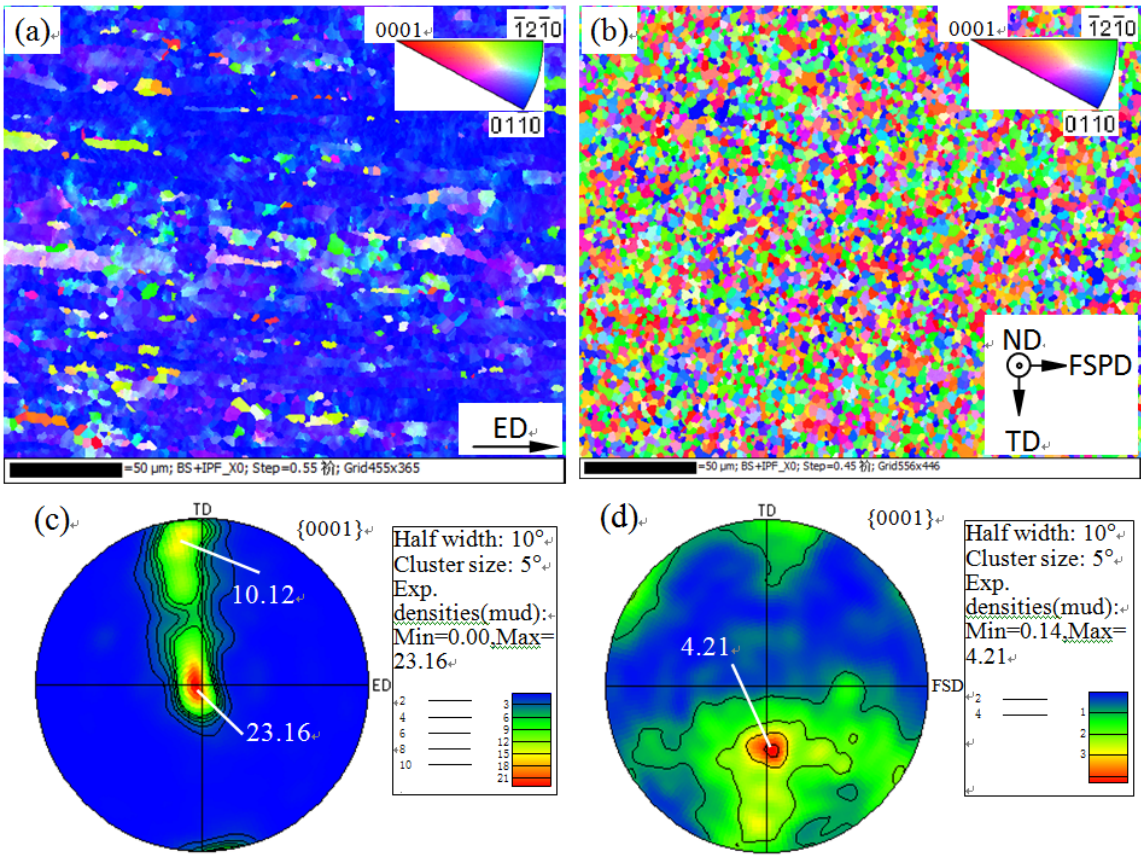

Fig. 7. Inverse pole figure (IPF) maps and {0001} pole figures (PFs) of (a-c) as-extruded alloys and (b-d) as-FSPed alloys

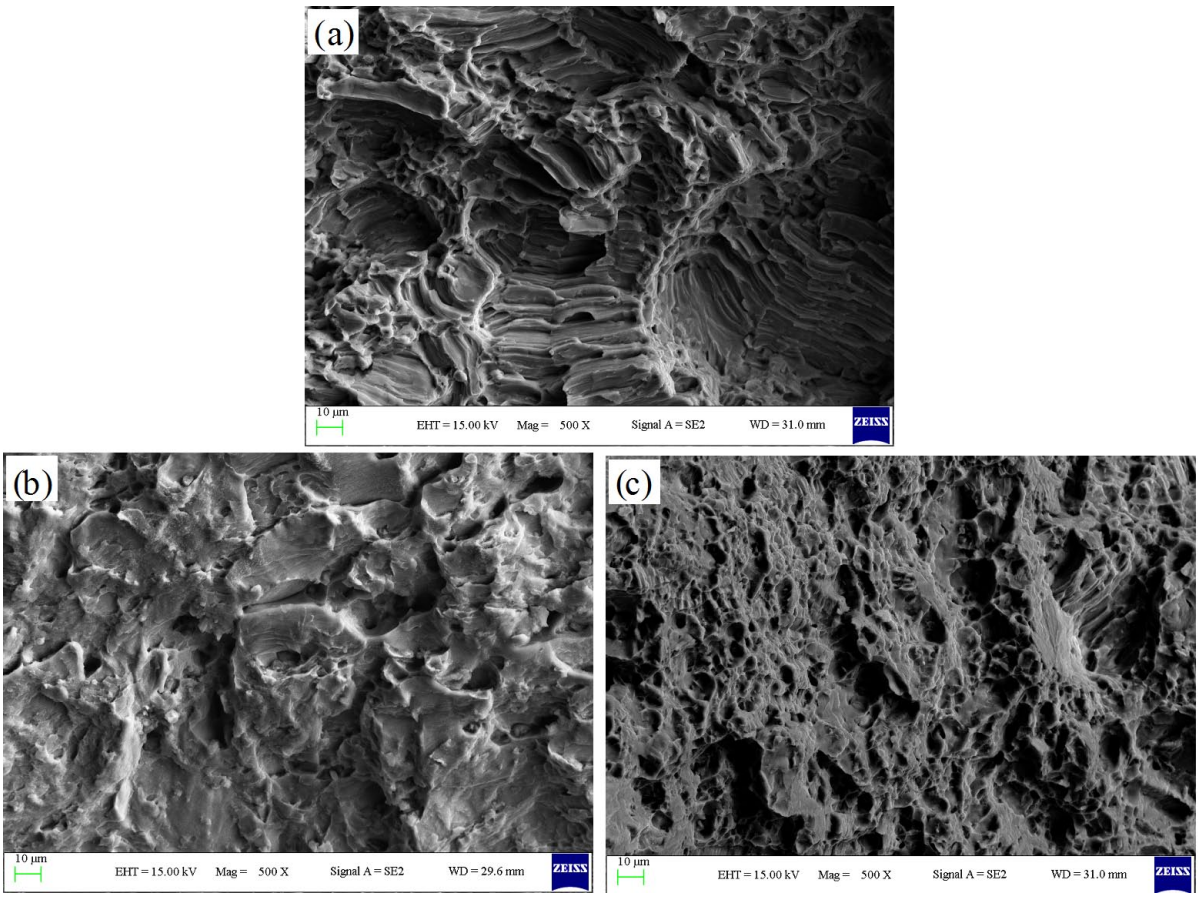

Fig. 8. SEM fractures morphologies of Mg-8Li alloy under different conditions after tensile (a) as-cast, (b) as-extruded and (c) as-FSPed

(2) The as-FSPed alloys showed superior performance with respect to the as-extruded samples. The YS, UTS and EL of the as-FSPed alloy reached 185.3 MPa, 235.4 MPa and 35.6%, respectively.

(3) The strengthening effect from the evolution of LAGBs and HAGBs during the processes of hot-extrusion and friction stir is the main underlying mechanism for the increase of yield stress of the Mg-Li alloy. And the extremely fine grains and high fraction of HAGBs play leading role in effectively improving the as-FSPed alloys' strength.

(4) The random texture in the as-FSPed alloys is the main mechanism responsible for the increased ductility of the alloy.

REFERENCES

[1] H.B. Ji, G.C. Yao, H.B. Li, J. Univ. Sci. Technol. B. **15** (4), 440-443 (2008).
DOI: https://doi.org/10.1016/S1005-8850(08)60083-3

[2] G. Liu, W. Xie, A. Hadadzadeh, G.B. Wei, Z.D. Ma, J.W. Liu, Y. Yang, W.D. Xie, X.D. Peng, M. Wells, J. Alloys Compd. **766**, 460-469 (2018).
DOI: https://doi.org/10.1016/j.jallcom.2018.07.024

[3] Y. Zou, L.H. Zhang, Y. Li, H.T. Wang, J.B. Liu, P.K. Liaw, H.B. Bei, Z.W. Zhang, J. Alloys Compd. **735**, 2625-2633 (2018).
DOI: https://doi.org/10.1016/j.jallcom.2017.12.025

[4] R.Z. Wu, Y.D. Yan, G.X. Wang, L.E. Murr, W. Han, Z.W. Zhang, M.L. Zhang, Int. Mater. Rev. **60** (2), 65-100 (2015).
DOI: https://doi.org/10.1179/1743280414Y.0000000044

[5] X.S. Fu, Y. Yang, J.W. Hu, J.F. Su, X.P. Zhang, X.D. Peng, Mater. Sci. Eng. A. **709**, 247-253 (2018).
DOI: https://doi.org/10.1016/j.msea.2017.10.036

[6] Z.L. Zhao, Z.W. Sun, W. Liang, Y.D. Wang, L.P. Bian, Mater. Sci. Eng. A.**702**, 206-217 (2017).
DOI: https://doi.org/ 10.1016/j.msea.2017.06.077

[7] L.R. Cheng, Z.Y. Cao, R.Z. Wu, M.L. Zhang, D.M. Jiang, Mater. Trans. **51** (9), 1526-1530 (2010).
DOI: https://doi.org/10.2320/matertrans.M2010156

[8] F. Mitsuaki, X. Cheng, A. Tetsuo ,I. Makoto, A. Hiroshi, T. Langdon, Mater. Sci. Eng. A. **410-411**, 439-442 (2005).
DOI: https://doi.org/10.1016/j.msea.2005.08.143

[9] W.J. Kim, Scr. Mater. **61** (6), 652-655 (2009).
DOI: https://doi.org/10.1016/j.scriptamat.2009.06.001

[10] H.J. Wu, T.Z. Wang, R.Z. Wu, L.G. Hou, J.H. Zhang, X.L. Li, M.L. Zhang, J. Mater. Process. Technol. **254**, 265-276 **(**2018).
DOI: https://doi.org/10.1016/j.jmatprotec.2017.11.033

[11] S. Feng, W.C. Liu, J. Zhao, G.H.Wu, H.H. Zhang, W.J. Ding, Mater. Sci. Eng. A. **692**, 9-16 (2017).
DOI: https://doi.org/10.1016/j.msea.2017.03.059

[12] A.M. Jamili, A.Z. Hanzaki, H.R. Abedi, P. Minárik, R. Soltani, Mater. Sci. Eng. A. **690**, 244-253 (2017).
DOI: https://doi.org/10.1016/j.msea.2017.02.096

[13] M. Narimani, B. Lotfi, Z. Sadeghian, Mater. Sci. Eng. A. **673**, 436-422 (2016).
DOI: https://doi.org/10.1016/j.msea.2016.07.086

[14] L.Q. Wang, L.H. Xie, P.Q. Shen, Q. Fan, W. Wang, K.S. Wang, W.J. Lu, L. Hua, L.C. Zhang, Mater. Charact. **153**, 175-183 (2019).
DOI: https://doi.org/10.1016/j.matchar.2019.05.002

[15] F.J. Liu, Y. Ji, Z.Y. Sun, J.B. Liu, Y.X. Bai, Z.K. Shen, J. Alloys. Compd. **829**, 154452 (2020).
DOI: https://doi.org/10.1016/j.jallcom.2020.154452

[16] J. Babu, M. Anjaiah, A. Mathew, Mater. Today Proc. **5** (2), 4515-4522 (2018).
DOI: https://doi.org/10.1016/j.matpr.2017.12.021

[17] E. Cerri, P. Leo, Mater. Sci. Forum **783** (2), 1735-1740 (2014).
DOI: https://doi.org/10.4028/www.scientific.net/MSF.783-786.1735

[18] X.Y. Chen, Y. Zhang, M.Q. Cong, Vacuum **175**, 109292 (2020).
DOI: https://doi.org/10.1016/j.vacuum.2020.109292

[19] Y. Zou, L.H. Zhang, Y. Li, H.T. Wang, J.B. Liu, P.K. Liaw, H.B. Bei, Z.W. Zhang, J. Alloy. Compd. **735**, 2625-2633 (2018).
DOI: https://doi.org/10.1016/j.jallcom.2017.12.025

[20] Q.Y. Che, K.S. Wang, W. Wang, L.Y. Huang, T.Q. Li, X.P. Xi, P. Peng, K. Qiao, Rare Metals **40** (9), 2552-2559 (2021).
DOI: https://doi.org/10.1007/s12598-019-01217-2

[21] L.Y. Jiang, W. Jiang, F. Guo, W.J. Huang, H.P. Dong, H.J. Hu, Q.W. Dai, Mater. Charact. **173**, 110979 (2021).
DOI: https://doi.org/10.1016/j.matchar.2021.110979

[22] S.S. Li, L. Chen, J.W. Tang, G.Q. Zhao, C.S. Zhang, Results Phys. **13**, 102148 (2019).
DOI: https://doi.org/10.1016/j.rinp.2019.02.084

[23] Y. Yang, X.M. Xiong, J.F. Su, X.D. Peng, H.M. Wen, G.B. Wei, F.S. Pan, E.J. Lavernia, J. Alloys Compd. **750**, 696-705 (2018).
DOI: https://doi.org/10.1016/j.jallcom.2018.03.319

[24] T.C. Xu, X.D. Peng, J.W. Jiang, W.D.Xie, Y.F. Chen, G.B. Wei, Trans. Nonferrous Met. Soc. China. **24** (9), 2752-2760 (2014).
DOI: https://doi.org/10.1016/S1003-6326(14)63406-3

[25] H.C. Pan, G.W. Qin, Y.M. Huang, Y.P. Ren, X.C. Sha, X.D. Han, Z.Q. Liu, C.F. Li, X.L. Wu, H.W. Chen, C. He, L.J. Chai, Y.Z. Wang, J.F. Nie, Acta Mater. **149**, 350-363 (2018).
DOI: https://doi.org/10.1016/j.actamat.2018.03.002

[26] J. Jain, P. Cizek, W.J. Poole, M.R. Barnett, Acta Mater. **61** (11), 4091-4102 (2013).
DOI: https://doi.org/10.1016/j.actamat.2013.03.033

[27] P. Luo, D.T. McDonald, W. Xu, S. Palanisamy, M.S. Dargusch, K. Xia, Scripta Mater. **66** (10), 785-788 (2012).
DOI: https://doi.org/10.1016/j.scriptamat.2012.02.008